crystals

MDPI

Review

Mechanisms of Pressure-Induced Phase Transitions by Real-Time Laue Diffraction

Dmitry Popov [1,*], Nenad Velisavljevic [1,2] and Maddury Somayazulu [1]

[1] High Pressure Collaborative Access Team, X-ray Science Division, Argonne National Laboratory, Lemont, IL 60439, USA; hpcat-director@anl.gov (N.V.); zulu@anl.gov (M.S.)

[2] Physics Division-Physical & Life Sciences Directorate, Lawrence Livermore National Laboratory, Livermore, CA 94550, USA

* Correspondence: dpopov@anl.gov

Received: 30 November 2019; Accepted: 11 December 2019; Published: 14 December 2019

Abstract: Synchrotron X-ray radiation Laue diffraction is a widely used diagnostic technique for characterizing the microstructure of materials. An exciting feature of this technique is that comparable numbers of reflections can be measured several orders of magnitude faster than using monochromatic methods. This makes polychromatic beam diffraction a powerful tool for time-resolved microstructural studies, critical for understanding pressure-induced phase transition mechanisms, by in situ and in operando measurements. The current status of this technique, including experimental routines and data analysis, is presented along with some case studies. The new experimental setup at the High-Pressure Collaborative Access Team (HPCAT) facility at the Advanced Photon Source, specifically dedicated for in situ and in operando microstructural studies by Laue diffraction under high pressure, is presented.

Keywords: Laue diffraction; high pressure; mechanisms of phase transitions

1. Introduction

White beam (polychromatic) Laue diffraction is a powerful experimental tool for studying mechanisms of pressure-induced phase transitions. Use of the full white beam spectrum allows for fast data collection, which then provides both spatially and time-resolved microstructural information to be gained simultaneously from a sample in Diamond Anvil Cell (DAC), with spatial resolution down to microns and time resolution down to seconds [1,2]. The alternative, using monochromatic beam diffraction, would not provide comparable time resolution, even with high X-ray energies, due to the need to rotate the sample while collecting X-ray images [3,4]. This makes total data collection time across the sample in a DAC substantially longer.

To some extent, the mechanisms of transitions can be determined by studying samples recovered at ambient pressure [5–7]. However, such samples may be substantially altered during the recovery process or undergo reversible phase transformations as pressure is released. In contrast, polychromatic beam diffraction makes it possible to determine the morphology, deformation and orientation relations of co-existing parental and product phases in real time in situ. Time-resolved measurements are vital for revealing details of phase transitions, which may be controlled by kinetics, and therefore require the fastest techniques of data collection.

Despite the fairly wide use of Laue diffraction for characterization of materials, including in situ studies of materials under external stress [8–10], the application of this technique for high-pressure DAC studies requires additional experimental development and consideration. The purpose of this review article is to summarize the currently available polychromatic beam diffraction experimental

techniques at high pressure and data analysis capabilities at HPCAT, as well as to present some recent case studies.

2. Experimental Facilities and Procedures

There are multiple synchrotron beamlines dedicated to Laue micro-diffraction [10–13]. However, currently these facilities are not specifically optimized for measurements on materials at high pressures. The first experimental setup specifically dedicated to high-pressure Laue micro-diffraction was developed at the 16BMB beamline of the Advanced Photon Source (APS) [2] (Figure 1). This setup is mounted on a granite table in order to maintain mechanical stability and positioning of the x-ray beam spot on the sample. A fast PerkinElmer area detector (PerkinElmer Optoelectronics) is positioned with a detector arm and, therefore, can be oriented in either transmitted or 90° geometry. The X-ray polychromatic beam from the bending magnet is focused down to 2μm^2 with KB-mirrors. The highest limit of X-ray energy at the sample position is adjustable by changing the tilt of the mirrors. For measurements in transmitted geometry, the highest possible energy is typically set at ~90keV, while in 90° geometry, the highest energy limit is around 35keV. The sample for high-pressure studies in a DAC is mounted on top of a fast x/y table, which in turn is mounted on top of an elevation stage. These stages are used to collect a series of two-dimensional (2D) translational scans across the sample. With a vertical rotational stage, sample orientation can be optimized to obtain the highest number of reflections. A Si 111 channel-cut monochromator provides monochromatic beam switchable with the polychromatic beam in a matter of minutes. This monochromatic beam is mainly used to identify powdered product phases after destructive phase transitions, to calibrate sample to detector distance and detector tilt in transmitted geometry using the CeO_2 standard. Detector calibration in 90° geometry is done using the Laue diffraction pattern from a Si single crystal and the known energy of one reflection on this pattern measured with the monochromator [14].

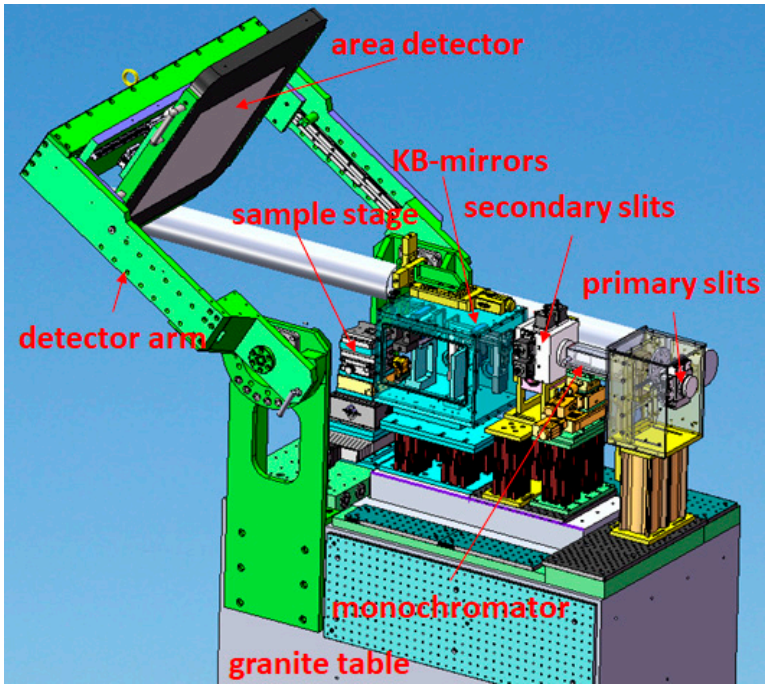

Figure 1. Outline of Laue diffraction setup dedicated to studies at high pressure available at 16BMB beamline of Advanced Photon Source [2].

Measurements in a DAC introduce some specific requirements to the sample environment (Figure 2). Strong Laue reflections from diamonds can damage the area detector. To protect the detector during data collection a detector mask is used: small pieces of lead are placed on a kapton foil in order

to block the reflections from the diamonds. Positions of strong diamond reflections are pre-determined by collecting an X-ray image with strong absorbers inserted in the incident beam to reduce intensities of these reflections to the level at which they will not damage the detector. A metal grid is placed on the kapton foil during the collecting of this image; this introduces a clear 'imprint' on the background of the pattern. Using the grid as a reference the pieces of lead are placed to the positions on the kapton foil coinciding with the strong diamond reflections. Before the detector mask is positioned, the sample is aligned in the X-ray beam and co-linear with the axis of the rotational stage by doing absorption scans across the sample with photodiode. A movable lead shield is used to protect the detector during this process and is removed for data collection.

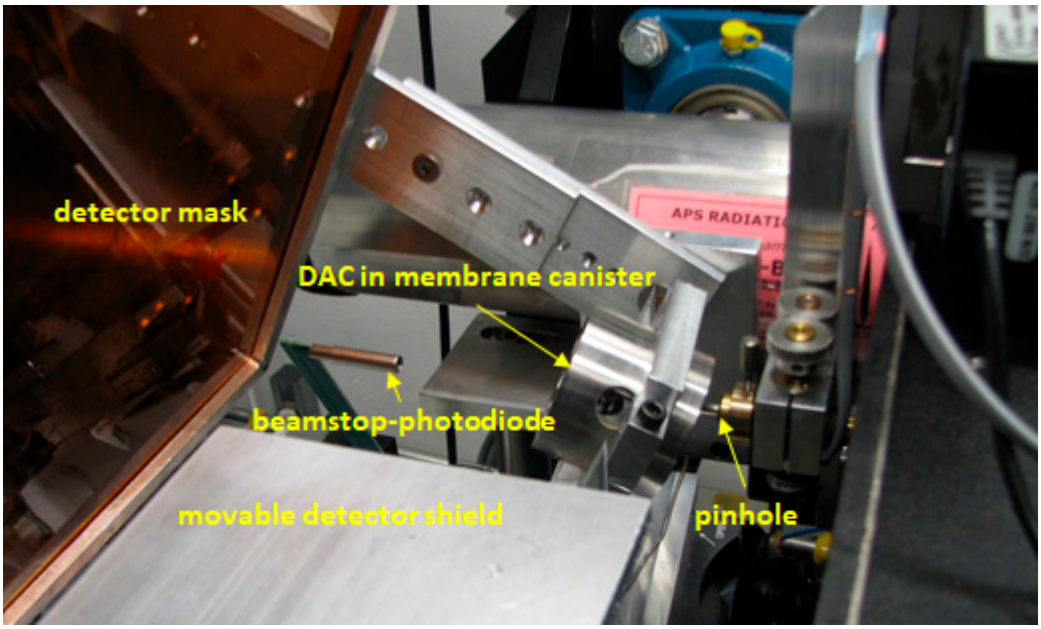

Figure 2. Sample environment of the Laue diffraction setup available at 16BMB beamline of Advanced Photon Source [2].

A series of 2D scans is collected across the sample undergoing a phase transition, while sample pressure is varied remotely using a gas membrane system. Microstructural changes during the transition are observed in real time using ImageJ software [15], and pressure can be fine-tuned based on the observed changes, such that the most important details of the transition are not lost. As the sample position may shift during pressure change, it has to be periodically re-centered on the rotation axis during data collection, in order to maintain a constant spatial sample-to-detector relationship. This procedure requires absorption scans across the sample at different angular positions of the sample [16,17]. Therefore, a detector mask is not sufficient to eliminate unwanted diffraction spots, and the movable detector shield is used instead. During the experiment, pressure is continuously monitored, and is also measured before and after the transition using an off-line Ruby fluorescence system [18] that is available inside the experimental hutch.

For the measurements in 90° geometry, a panoramic DAC with X-ray transparent gasket is used. The incident beam passes through the diamond, while the diffracted beams pass through the gasket material. In transmitted geometry, both incident and diffracted beams pass through diamonds. For the measurements in this configuration typically DACs with total opening of ~60° are used. The DACs are tilted vertically by ~25° with a sample holder, and the area detector is tilted vertically by 30°. This configuration optimizes the amount of reciprocal space that can be accessed and allows us to collect sufficient number of reflections for indexing them.

Phase transitions may proceed very rapidly, and in order to observe details of phase transitions, pressure has to be changed in small steps. In the case of strongly displacive transitions, the initial

parent single crystal sample breaks up into smaller crystals or powder-like crystalline aggregates. Due to this process, the sample becomes heavily deformed, which introduces additional difficulties in data analysis. In practice, one must therefore follow the process until this deformation sets in and makes analysis difficult. Using Re gaskets in the transmitted geometry currently pressure rate can be as small as ~0.2 GPa/hour and can therefore allow us to appropriately capture the transition.

Measurements in diamond anvil cells require sufficiently small samples, typically smaller than 100 μm. Therefore, if the sample is bigger, a small part has to be separated from it. On the other hand, Laue diffraction is sensitive only to single crystals with sizes comparable to or larger than X-ray beams, so the original samples must be either single crystals or poly crystals with crystal size typically at least in the micron range. If the sample is too big to be put into a DAC but it is a single crystal with strong cleavage, it can be mechanically split into smaller crystals that still have good quality for the measurements. However, if the mechanical disintegration of the sample destroys the single crystals, an alternative approach may be considered using a laser micro-machining system [19]. The sufficiently small sample is carefully put in the center of gasket hole of a DAC using Axis Pro Micro Support micromanipulator (Supplementary Materials, Figure S1). Positioning of the sample right in the center of gasket hole is crucial to minimize diffraction signal from gasket material and to avoid sample-gasket interaction during pressure changes.

3. Data Analysis

Analysis of the high-pressure Laue diffraction data includes two major steps: indexation of diffraction patterns [14,20], and mapping of reflections. By systematic indexing of diffraction spots, single crystals can be identified, and therefore reflections from parent and daughter phases can be clearly distinguished. Furthermore, by going through systematic indexation, orientations of crystals can be determined, which in turn can be used to find orientation relations between coexisting parent and product phases. Relative orientations of single crystals can be determined from one Laue diffraction pattern with an angular precision down to ~0.02°, which makes Laue diffraction a powerful tool for characterizing twining [21]. By application of the polychromatic beam diffraction, one can overcome a major challenge to recognize domain structures formed after phase transitions: the newly formed domains typically have pseudo symmetrical translational lattices with very low mismatch with respect to the lattice of parental phase [22]. As a Laue diffraction pattern is typically collected in a matter of a few seconds, such domain structures can be recognized in real time with a resolution reaching down to seconds. At the same time, determining twin relationships with the same level of precision using a monochromatic beam requires sample rotations in very small steps and correspondingly large data collection times.

Software for indexing and mapping of Laue reflections was developed in-house by the lead author of this paper D. Popov, in Python [23]. This program can be made available upon request, as it is developed for broader distribution. The indexation routine is tailored toward simultaneous indexation of reflections from multiple crystals or crystallites that can coexist on the same diffraction pattern. Two strong diffraction spots that could belong to the same crystal are selected first. Typically, two reflections from the same 'zone line' are selected, which is a good indication that reflections originate from the same crystal. Based on the positions of these diffraction spots and their indices, the orientation matrix of the crystal can be calculated [20]. However, in many cases, the indices are not known, and therefore the software is used to explore and converge on the possible indices for calculating the orientation matrix and indexing all other reflections using this matrix. Orientation matching to substantially bigger number of reflections than multiple orientations is first exhausted. The range of possible indices is determined based on 2θ angles of the selected two reflections and the highest limit of X-ray energy. After the diffraction spots from a crystal are determined, they are removed from further data analysis, and reflections from other crystals are indexed in the same repetitive way. The peak search function available in Fit2d [24] software is used for determining the positions of reflections.

The newly developed program can even detect a rather unlikely situation in which the same set of reflections can be indexed by multiple crystal orientations. In such a case, the data has to be recollected in order to obtain a broader set of reflections from the sample. A larger set of reflections can typically be obtained by using DACs with larger openings, varying sample orientation, and reducing the sample-to-detector distance. For example, one should avoid situations where only one 'zone line' from a crystal is present in the diffraction pattern, since, in those cases, there are two possible orientation variants that satisfy the diffraction condition. These two orientations are related by a mirror plane perpendicular to the zone axis.

Crystal orientation is determined from reflections picked up on X-ray images using a peak search algorithm which may not be able to recognize all diffraction spots. More reliably, all the reflections from a single crystal can be visually recognized. For this purpose, positions of all possible reflections from a single crystal are predicted and shown on X-ray image, by the new program, based on orientation matrix, highest X-ray energy limit, and some lower limit of d-values (Figure 3a). Software Dioptas [25], widely implemented in the high-pressure area, is used to visualize X-ray images with marks of predicted reflection positions and to look through series of such diffraction patterns collected during a 2D scan.

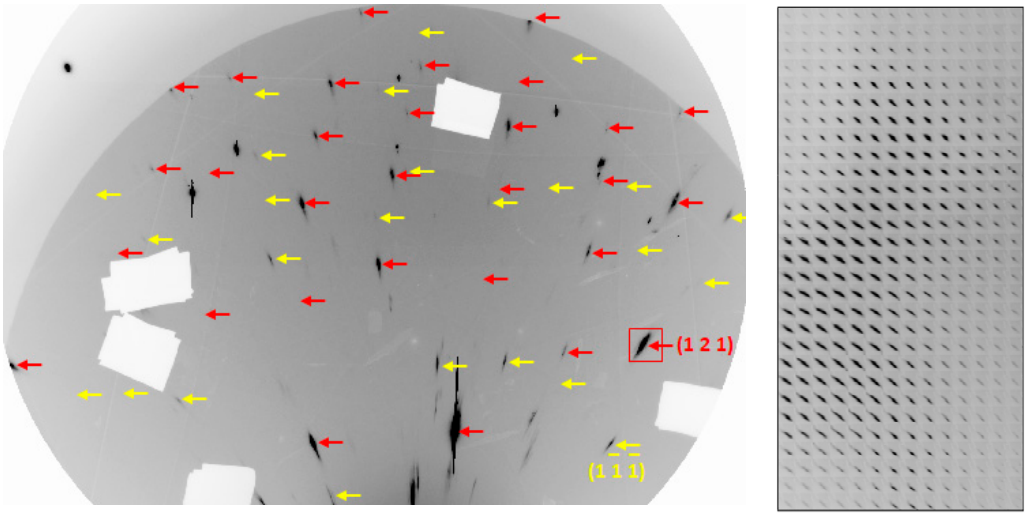

(**a**) (**b**)

Figure 3. Results of identification and mapping of two ω-Zr crystals using Laue diffraction data collected at 34IDE beamline of APS with X-ray beam focused down to 500×500nm^2 at pressure of 5.16GPa. (**a**) Predicted positions of reflections from the two crystals of ω-Zr (shown by different colors, slightly shifted to the right not to overlap with the observed reflections) on a Laue diffraction pattern assuming X-ray energy limit of 30keV and the smallest d-values of 0.55Å (positions shown in red) and 0.65Å (positions shown in yellow). (**b**) Composite frame of area denoted by red rectangle in (**a**) presenting a map of (121) reflection. Composite frames of areas around some other reflections from the same crystal are presented in the Supplementary Materials (Figure S2).

For mapping the single crystal, the new program combines all images collected during the 2D scan of the crystal into a composite frame in the same order as those images were collected during the scan (Figure 3b). Such composite frames reproduce the shapes of single crystals and, at the same time, variations in the shapes and positions of diffraction spots across the sample are also clearly visible, indicating deformation of the crystals. The composite images are currently visualized with Fit2d.

In general, the microstructural changes during phase transitions are continuous, and as such, in order to analyze the 2D scans, one has to distinguish between changes that could be attributed to spatial inhomogeneity of the sample and those caused by temporal changes during the transition.

Typically, there is variation in the diffraction spot positions across both the parental and product single crystals caused by their deformation. At the same time, rotation of the crystals due to deformation of the entire sample during a translational scan causes such a variation as well. Pressure increase may slightly mis-orient the DAC during a translational scan, also resulting in variation of diffraction spot positions across the single crystals. The shapes of diffraction spots may also vary across parent crystals coexisting with product phase due to the inhomogeneity of their deformation. However, if the crystals are deformed during a 2D translational scan, they exhibit the same kind of variation. Maps of reflections across the sample are defined by crystal morphology, but the maps can also be affected by decreasing parent fraction or growth of product phase during the scan. The variations due to sample inhomogeneity are distinguished by comparing concurrent translational scans in order to find reproducible features. For instance, the composite frame presented in Figure 3b was extracted from a scan repeated twice. The composite frame from the second scan is identical, indicating that there were no observable changes in the sample within the time interval of 12 h required to collect both of the scans. Therefore, the composite frame clearly reproduces the shape of the crystal, and no changes to its morphology are indicated. More composite frames of reflections from the same crystal are presented in Supplementary Materials (Figure S2).

4. Examples

The mechanism of the $\alpha \rightarrow \beta$ transition in Si was studied using Laue diffraction [1]. In Figure 4, maps of coexisting parent and product phases at the onset of transition are presented (Figure 4a), along with map of the rest of parent α-Si single crystal (Figure 4b).

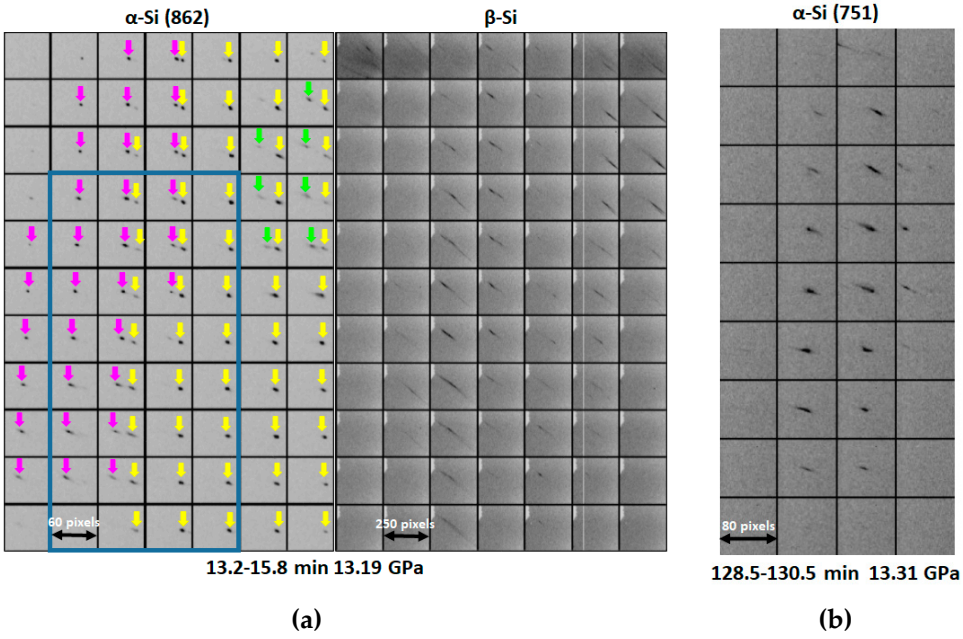

Figure 4. Maps of the parent and product phases across the $\alpha \rightarrow \beta$ phase transition in Si [1]. Time intervals of the 2D scans since the beginning of the data collection routine are shown. The pressure values have been interpolated based on the pressures measured before and after the transition. Step size was 5 µm. (**a**) Composite frames of reflections from three slightly mis-oriented crystals of α-Si (shown in different colors) and β-Si. The blue rectangle denotes the overlap area with the map presented in (**b**). (**b**) Map of the rest of parent α-Si crystal when the transition was nearly over.

Microstructural changes that evolve over longer time periods in comparison to typical acquisition times of one translational scan can be better analyzed and viewed by combining composite frames from consecutive scans. As examples, movies (Movie S1a,b) compiled from composite frames shown in Figure 4 are presented in the Supplementary Materials. Movie S1a captures the splitting of the

original single crystal of α-Si at the onset of transition into three crystals that are slightly mis-oriented with respect to one another, while the newly formed β-Si is located at the interface of these crystals. In Movie S1b, the disintegration of the rest of parental single crystal is shown.

The results of study of the mechanism of the α → β phase transition in Si [1] presented in Movie S1a indicate that the interface between the parental and product phases is highly incoherent. While the α-phase produced very sharp reflections, the β-phase produced highly broadened 'streaky' reflections, indicating that crystals of this phase were heavily deformed. Most likely, this is due to the large volume collapse accompanying this transition, which then resulted in large lattice mismatch between the parent and daughter phases. The areas of β-Si were strongly elongated domains formed parallel to a <110> direction of the parent α-Si phase. This may also indicate that the nucleation of the product phase could be controlled by defects introduced along the cleavage planes during the sample preparation. It is interesting to note that the single crystals of α-Si were slightly bent as the β-phase started growing. This is indicated by the systematic shift of positions of reflections from α-Si across the sample reproducible on the composite frames from adjacent translational scans. Toward the end of the transition, the rest of the parental single crystal also exhibited the same kind of deformation (Movie S1b). The remaining α-Si crystal was strongly elongated parallel to the same <110> direction as the β-Si areas on the onset of transition.

Another example is our recent study of zirconium (Zr) metal. Zr has previously been observed to exhibit unusual grain enlargement across the α → ω phase transition [26]. The parent phase is a nano-crystalline aggregate, while the product phase is much grainier. The relative change in grain size structure was inferred from the 'spotty' diffraction lines recorded with a monochromatic beam on the daughter ω-phase of Zr in comparison to the continuous diffraction lines from the parent α-phase of Zr. The grain enlargement in Zr is observed under high pressure and room temperature conditions, as opposed to typical grain enlargement processes that are required to occur at elevated temperatures to overcome the activation barriers for diffusion. Currently, both the driving force and the mechanism of this phenomenon remain unknown. Measurements with a polychromatic beam that is 500 × 500 nm^2 size demonstrated that the newly formed ω-Zr crystals may have an irregular morphology (Figure 3b).

Using Laue diffraction, the grain enlargement process in Zr was studied in real time [27]. Initially, we did not observe any Laue reflections from the fine-grained parent α-phase. As Zr started to undergo a transition to ω-phase, we started to observe the appearance of strong diffraction spots. The intensities of these reflections increased gradually along with increasing pressure. Mapping of the ω-Zr reflections clearly demonstrated that the ω-Zr crystals nucleated and grew in the nano-crystalline matrix of α-Zr. In the Supplementary Materials, a movie combined from maps of an ω-Zr reflection is presented as an example (Movie S2). The sizes of the newly formed ω-Zr crystals gradually increased along with the increase in pressure, while the intensities of the ω-Zr reflections gradually decreased towards the edges of the crystals away from the nucleation points. These observations indicate a grain enlargement mechanism that involves formation and movement of highly angular grain boundaries, distinguishing the enlargement from a recovery process in which stored energy of dislocations is released without movement of the grain boundaries. In the case of recovery, intensities of ω-Zr reflections on the composite frames would increase simultaneously over a single grain area. This is followed by gradual sharpening of the ω-Zr reflections. The observed ω-Zr reflections stayed at the same level of broadening during the grain enlargement process indicating that there was no substantial texture development involved in this process. The majority of ω-Zr reflections exhibited only positive shifts of their intensities, indicating that ω-Zr crystals mainly grew at a cost to α-phase, and not at cost to each other, as would be the case if the enlargement process had a similar nature to the widely known grain coarsening process.

5. Future Developments

In the future, faster area detectors and translational stages will be implemented in order to improve the time resolution of this technique, while improvement of its spatial resolution will require smaller

incident beams. Improvement of both spatial and time resolution will provide better details of the phase transition mechanisms and interface developments thereof. For example, implementation of X-ray polychromatic beams focused down below 100 nm [12] may provide details of the mechanism of the pressure induced grain enlargement observed across the $\alpha \rightarrow \omega$ phase transition in Zr.

A clear advantage of DAC compared to other stress generation devices is that the sample can be studied under hydrostatic compression or alternately under shear. Hydrostatic pressure using either He or Ne as a transmitting medium can be contrasted with studies with other media (such as silicone oil for example), thereby modifying the shear forces.

Supplementary Materials: The following are available online at http://www.mdpi.com/2073-4352/9/12/672/s1, Figure S1: Axis Pro Micro Support micromanipulator available in sample preparation laboratory of HPCAT, Figure S2: maps of reflections (indices are shown) from a crystal of ω-Zr, Movies S1a and S1b: series of composite frames of reflections from coexisting α- and β-Si [1] at the onset of $\alpha \rightarrow \beta$ transition (S1a) and when the transition was nearly over (S1b), arrows of different colors in S1a denote reflections from different crystals of α-Si, rectangle in S1a denotes overlap area with S1b, Movie S2: series of composite frames of a reflection from an ω-Zr crystal growing during the $\alpha \rightarrow \omega$ transition [27], time intervals since starting of data collection are shown in the movies.

Author Contributions: Conceptualization, D.P. and N.V.; software, D.P.; writing—original draft preparation, D.P. and N.V.; writing—review and editing, M.S.

Funding: This research was funded by DOE-NNSA's Office of Experimental Sciences. The Advanced Photon Source was funded by the U.S. Department of Energy (DOE) Office of Science.

Acknowledgments: This work was performed at HPCAT (Sector 16), Advanced Photon Source (APS), Argonne National Laboratory. HPCAT operations are supported by DOE-NNSA's Office of Experimental Sciences. The Advanced Photon Source is a U.S. Department of Energy (DOE) Office of Science User Facility operated for the DOE Office of Science by Argonne National Laboratory under Contract No. DE-AC02-06CH11357. Part of this work was performed under the auspices of the U.S. Department of Energy by Lawrence Livermore National Laboratory under Contract DE-AC52-07NA27344.

Conflicts of Interest: The authors declare no conflict of interest.

References

1. Popov, D.; Park, C.; Kenney-Benson, C.; Shen, G. High pressure Laue diffraction and its application to study microstructural changes during the α→β phase transition in Si. *Rev. Sci. Instrum.* **2015**, *86*, 072204. [CrossRef] [PubMed]
2. Popov, D.; Sinogeikin, S.; Park, C.; Rod, E.; Smith, J.; Ferry, R.; Kenney-Benson, C.; Velisavljevic, N.; Shen, G. New Laue micro-diffraction setup for real-time in situ microstructural characterization of materials under external stress. In *Advanced Real Time Imaging II. The Minerals, Metals & Materials Series*; Nakano, J., Chris Pistorius, P., Tamerler, C., Yasuda, H., Zhang, Z., Dogan, N., Wang, W., Saito, N., Webler, B., Eds.; Springer: Cham, Germsny, 2019; pp. 43–48. [CrossRef]
3. Shen, G.; Mao, H.K. High-pressure studies with x-rays using diamond anvil cells. *Rep. Prog. Phys.* **2017**, *80*, 016101. [CrossRef] [PubMed]
4. McMahon, M.I. High-pressure crystallography. *Top. Curr. Chem.* **2012**, *315*, 69–110. [CrossRef] [PubMed]
5. Lorenz, H.; Lorenz, B.; Kuhne, U. The kinetics of cubic boron nitride formation in the system BN-Mg_2N_2. *J. Mater. Sci.* **1988**, *23*, 3254–3257. [CrossRef]
6. Dupas-Bruzek, C.; Sharp, T.G.; Rubie, D.C.; Durham, W.B. Mechanisms of transformation and deformation in $Mg_{1.8}Fe_{0.2}SiO_4$ olivine and wadsleyite under non-hydrostatic stress. *Phys. Earth Planet. Inter.* **1998**, *108*, 33–48. [CrossRef]
7. Kerschhofer, L.; Rubie, D.C.; Sharp, T.G.; McConnell, J.D.C.; Dupas-Bruzek, C. Kinetics of intracrystalline olivine–ringwoodite transformation. *Phys. Earth Planet. Inter.* **2000**, *121*, 59–76. [CrossRef]
8. Ice, G.E.; Pang, J.W.L. Tutorial on x-ray microLaue diffraction. *Mater. Charact.* **2009**, *60*, 1191–1201. [CrossRef]
9. Cornelius, T.W.; Thomas, O. Progress of in situ synchrotron X-ray diffraction studies on the mechanical behavior of materials at small scales. *Prog. Mater. Sci.* **2018**, *94*, 384–434. [CrossRef]
10. Robach, O.; Kirchlechner, C.; Micha, J.S.; Ulrich, O.; Biquard, X.; Geaymond, O.; Castelnau, O.; Bornert, M.; Petit, J.; Berveiller, S.; et al. Laue microdiffraction at the ESRF. In *Strain and Dislocation Gradients from Diffraction*; Barabash, R., Ice, G., Eds.; Imperial College Press: London, UK, 2014; pp. 156–204.

11. Ulrich, O.; Biquard, X.; Bleuet, P.; Geaymond, O.; Gergaud, P.; Micha, J.S.; Robach, O.; Rieutord, F. A new white beam x-ray microdiffraction setup on the BM32 beamline at the European Synchrotron Radiation Facility. *Rev. Sci. Instrum.* **2011**, *82*, 033908. [CrossRef] [PubMed]
12. Liu, W.; Ice, G.E. X-ray Laue diffraction microscopy in 3D at the Advanced Photon Source. In *Strain and Dislocation Gradients from Diffraction*; Barabash, R., Ice, G., Eds.; Imperial College Press: London, UK, 2014; pp. 53–81.
13. Tamura, N.; Kunz, M.; Chen, K.; Celestre, R.S.; MacDowell, A.A.; Warwick, T. A superbend X-ray microdiffraction beamline at the advanced light source. *Mater. Sci. Eng. A* **2009**, *524*, 28–32. [CrossRef]
14. Tischler, J.Z. Reconstructing 2D and 3D X-ray orientation maps from white-beam Laue. In *Strain and Dislocation Gradients from Diffraction*; Barabash, R., Ice, G., Eds.; Imperial College Press: London, UK, 2014; pp. 358–375.
15. ImageJ. Available online: https://imagej.nih.gov/ij/ (accessed on 12 December 2019).
16. Smith, J.S.; Desgreniers, S. Selected techniques in diamond anvil cell crystallography: Centring samples using X-ray transmission and rocking powder samples to improve X-ray diffraction image quality. *J. Synchrotron Radiat.* **2009**, *16*, 83–96. [CrossRef] [PubMed]
17. Smith, J.S.; Rod, E.A.; Shen, G. Fly scan apparatus for high pressure research using diamond anvil cells. *Rev. Sci. Instrum.* **2019**, *90*, 015116. [CrossRef]
18. Mao, H.K.; Xu, J.; Bell, P.M. Calibration of the Ruby pressure gauge to 800-kbar under quasi-hydrostatic conditions. *J. Geophys. Res. Solid Earth* **1986**, *91*, 4673–4676. [CrossRef]
19. Hrubiak, R.; Sinogeikin, S.; Rod, E.; Shen, G. The laser micro-machining system for diamond anvil cell experiments and general precision machining applications at the High Pressure Collaborative Access Team. *Rev. Sci. Instrum.* **2015**, *86*, 072202. [CrossRef] [PubMed]
20. Chung, J.S.; Ice, G.E. Automated indexing for texture and strain measurement with broad-bandpass x-ray microbeams. *J. Appl. Phys.* **1999**, *86*, 5249–5255. [CrossRef]
21. Barabash, R.; Barabash, O.; Popov, D.; Shen, G.; Park, C.; Yang, W. Multiscale twin hierarchy in NiMnGa shape memory alloys with Fe and Cu. *Acta Mater.* **2015**, *87*, 344–349. [CrossRef]
22. Hahn, T.; Klapper, H. Twinning of crystals. In *International Tables for Crystallography*, 2nd ed.; Chapter, 3.3; Authier, A., Ed.; John Wiley and Sons Limited: Hoboken, NJ, USA, 2013; Volume D, pp. 413–487. [CrossRef]
23. Python. Available online: https://www.python.org/ (accessed on 12 December 2019).
24. Hammersley, A.P.; Svensson, S.O.; Hanfland, M.; Fitch, A.N.; Hausermann, D. Two-dimensional detector software: From real detector to idealized image or two-theta scan. *J. High Press. Res.* **1996**, *14*, 235–248. [CrossRef]
25. Prescher, C.; Prakapenka, V. DIOPTAS: A program for reduction of two-dimensional X-ray diffraction data and data exploration. *J. High Press. Res.* **2015**, *35*, 223–230. [CrossRef]
26. Velisavljevic, N.; Chesnut, G.N.; Stevens, L.L.; Dattelbaum, D.M. Effects of interstitial impurities on the high pressure martensitic α to ω structural transformation and grain growth in zirconium. *J. Phys. Condens. Matter* **2011**, *23*, 125402. [CrossRef] [PubMed]
27. Popov, D.; Velisavljevic, N.; Liu, W.; Hrubiak, R.; Park, C.; Shen, G. Real time study of grain enlargement in zirconium under room-temperature compression across the α to ω phase transition. *Sci. Rep.* **2019**, *9*, 15712. [CrossRef] [PubMed]